

Optical probing of Rayleigh wave driven magneto-acoustic resonance

P. Kuszewski,¹ J.-Y. Duquesne,¹ L. Becerra,¹ A. Lemaître,² S. Vincent,¹ S. Majrab,¹ F. Marguillan,¹ C. Gourdon,¹ and L. Thevenard¹

¹*Sorbonne Université, CNRS, Institut des Nanosciences de Paris, 4 place Jussieu, 75252 Paris France*

²*Centre de Nanosciences et de Nanotechnologies, CNRS,*

Univ. Paris-Sud, Université Paris-Saclay, 91460 Marcoussis, France

(Dated: July 2, 2018)

The resonant interaction of electrically excited travelling surface acoustic waves and magnetization has been hitherto probed through the acoustic component. In this work it is investigated using time-resolved magneto-optical detection of magnetization dynamics. To that end, we develop an experimental scheme where laser pulses are used both to generate the acoustic wave frequency and to probe magnetization dynamics thus ensuring perfect phase locking. The light polarization dependence of the signal enables to disentangle elasto-optic and magneto-optic contributions and to obtain the in-plane and out-of-plane dynamic magnetization components. Magnetization precession is proved to be driven solely by the acoustic wave. Its amplitude is shown to resonate at the same field at which we detect piezo-electrically the resonant attenuation of the acoustic wave, clearly evidencing the magneto-acoustic resonance with high sensitivity.

I. INTRODUCTION

The recent years have witnessed a renewed and growing interest in the use of acoustic waves to excite spin waves as an alternative, fast, efficient, and heat-free means to generate and control (possibly coherently and remotely) information in magnetic materials^{1–16}. Magnetization switching^{3,7,11,12,16}, and parametric excitation of spin waves^{9,13} have for instance been demonstrated, thus opening new perspectives for applications. The efficiency of acoustic waves relies on magneto-elastic coupling that occurs in magnetostrictive materials. Static strain contributes to magnetic anisotropy^{17,18} whereas dynamic strain (acoustic waves) exerts a torque on the magnetization leading to precessional motion predicted to be resonantly enhanced when the spin wave frequency matches the acoustic wave frequency^{19,20}.

Among the various acoustic waves, propagating surface acoustic waves (SAW), such as Rayleigh waves, with typical frequencies up to the GHz range and dynamical strain component confined within a few μm from the surface, are particularly well suited to excite magnetization dynamics in thin ferromagnetic layers on a substrate. SAWs are easy to implement thus finding applications in various fields of soft and condensed matter physics^{21–24}. They can be generated either optically via thermoelasticity^{5,10,13,25} or electrically via the piezoelectric effect using interdigitated transducers (IDTs)²⁶. Since electrically generated SAWs are a well-mastered technology in microelectronics, SAW-induced magnetization control could be readily implemented in logic or memory devices, with the unprecedented possibility to use wave physics tools such as focusing, diffraction, and wave-guiding to address a magnetic bit.

In ferromagnetic systems, interaction of electrically generated SAWs with magnetization was evidenced by piezo-electrical detection after propagation of the SAW on the sample surface^{1,4}. The SAW amplitude and veloc-

ity resonantly decreased when the frequency of magnetization precession was varied through the SAW frequency by an applied magnetic field. By analogy with cavity-ferromagnetic resonance (FMR) this is known as SAW-FMR. However, magnetization precession has not been concomitantly observed although time-resolved detection of magneto-optical effects using probe laser pulses could provide a direct and most sensitive method to access magnetization dynamics²⁷. This requires a non-trivial synchronization of the SAW generation with probe laser pulses. This difficulty has been up to now bypassed by utilizing optically generated stationary SAWs^{5,10}. Very recently, synchrotron X-ray probe pulses were locked to electrically generated SAWs to investigate strain-driven modes in patterned ferromagnetic samples²⁸. No (resonant) magnetization dynamics were observed however.

In this article, we demonstrate the forced magnetic precession induced by *travelling* SAW bursts, using a table-top optical set-up. To that end we implement an innovative and simple way to generate electrically SAW bursts by IDTs with perfect phase locking to laser pulses, which allows the optical investigation of time- and space-resolved magnetization dynamics excited by the SAW. We illustrate the potentiality of this technique with a ferromagnetic semiconductor layer of GaMnAs on piezoelectric GaAs, taking advantage of its low FMR frequency easily tunable across the SAW frequency, and sizable magneto-optical effects. Using the probe light polarization and the magnetic field dependencies of the time-resolved signal we separate the magneto-optical from the pure elasto-optical contribution. The in-plane and out-of plane magnetization dynamical components display the predicted dependencies on the magnetic field. Finally, we show that resonant magnetic excitation appears concomitantly with resonant SAW absorption, the detection of the former being more sensitive than the latter.

II. EXPERIMENTAL SETUP

The simplest IDT consists of two comb-shaped electrodes in zipper configuration, that work as capacitors on a piezoelectric surface. When a radio-frequency (RF) voltage at f_{SAW} is applied, SAWs are generated and propagate on either side of the IDT. The wavelength λ_{SAW} of the excited SAW is determined by the period of the electrode teeth. Frequency and wavelength are related by $\lambda_{SAW} = \frac{v_R}{f_{SAW}}$ where v_R is the Rayleigh velocity. Typical λ_{SAW} values are around a few microns. The strain components excited with the IDT are: longitudinal ε_{xx} ($x \parallel \mathbf{k}_{SAW}$), transverse ε_{zz} (z perpendicular to the surface) and shear ε_{xz} (negligibly small close to the surface)²⁶. In more sophisticated IDT architectures it is possible to excite overtone harmonics of the fundamental frequency, such as the split-52 design²⁹, which is used in this work. Optical time-resolved measurement of magnetization dynamics requires a fixed phase between the laser pulses and the acoustic bursts. The most common solution is a phase-locked loop³⁰. The ‘master’ clock imposes the repetition rate of the ‘slave’ laser. The laser cavity length is continuously adjusted in order to meet the set frequency. We propose a simpler, elegant, and low-cost alternative approach where f_{SAW} is built from the laser repetition rate thereby ensuring a stable phase lock. Two research groups have very recently reported independently similar synchronization methods^{28,31}.

In order to generate the SAW RF frequency, a small fraction of a Ti:Sapphire laser at ~ 75 MHz repetition rate (f_L) was directed to a Silicon photodiode (Thorlabs PDA10A-EC, bandwidth 150 MHz) to pick up the laser fundamental frequency (Fig. 1(a)). Using different RF multipliers, multiples of the laser frequency were then generated: $n f_L$, where $n = 2, 4, 6, 8$. To ensure that $n f_L$ is free of any harmonics, the signal was filtered with 50 dB rejection band pass filters. The signal level was adjusted with a linear 40 dB amplifier and a set of attenuators.

The larger fraction of the 130 fs laser pulses (wavelength 722 nm) was sent to a pulse selector (Fig. 1(a)). The repetition rate was reduced by a factor 300 to $f_{rep} = 250$ kHz. This beam was used to probe the magnetization and strain dynamics in a time window of 12 ns controlled with a motorized optical delay line stage.

As we shall see hereafter the IDT needs to be fed with a pulsed RF signal. In order to fabricate these pulses the $n f_L$ CW RF signal was mixed with a 400 ns-wide rectangular pulse train from a pulse generator (Keysight 81150A) at the pulse picker frequency f_{rep} thus ensuring that both the envelope frequency and the RF frequency of the SAW are commensurate with f_L . With the pulse generator we could modify the burst duration and its arrival time (electronic delay) to the transducer. The ‘edge-to-reference’ jitter³² defined as the timing variation between the rising edge of the rectangular pulse and the optical pulse shows a standard deviation $\sigma = 13.1$ ps comfortably below 1% of the highest SAW period.

The linearly polarized laser pulses at f_{rep} were focused on the sample surface with a long working distance objective lens with numerical aperture 0.4. The laser beam reflected off the sample traveled through the same objective. The polarization rotation induced by the dynamical magnetization and strain components was detected by a balanced optical bridge relying on magneto-optical effects^{27,33} and the photo-elastic (PE) effect²⁶, respectively. The bridge output was demodulated by a lock-in amplifier at the frequency of a mechanical chopper $f_{ch} = 541$ Hz inserted on the laser beam before the slow photodiode (Fig. 1(a)), *i.e.* modulating the excitation SAW. Polarization rotations as small as 0.1 μ rad can routinely be measured.

The sample was a 45 nm thick, in-plane magnetized $\text{Ga}_{0.95}\text{Mn}_{0.05}\text{As}$ layer on a (001) GaAs substrate, annealed for 16 h at 200°C, with a Curie temperature $T_C = 120$ K. It was placed in an Oxford MicroStat HiRes cryostat that ensures the required mechanical stability and optical access. The GaMnAs layer has a strong uniaxial magnetic anisotropy with the easy axis along [1-10] and exhibits a large magneto-elastic coupling¹⁶. An in-plane magnetic field aligned with the hard axis [110] was applied to decrease the precession frequency and make it cross the SAW frequency. A 2x2 mm² square mesa of GaMnAs was prepared by chemical etching. At two opposite ends a set of 42 nm thick Aluminum IDTs with 1 mm aperture were deposited on the GaAs (Fig. 1(a)). In order to provide efficient operation of the IDTs even when varying the temperature (given the temperature dependence of $v_R(T)$) and to achieve a compromise between excitation efficiency and bandwidth, the IDTs were designed as 25 pairs of split-52 electrodes. With a digit width and inter-digit spacing of 1.9 μ m, the fundamental period was $\lambda_{SAW} = 19$ μ m. This ensured that the wavelength of all excited SAW frequencies was substantially larger than the laser spot diameter (full-width at half maximum of about 1 μ m). The RF voltage applied to the IDT triggers the propagation of a SAW along the [1-10] axis. The RF power was set to 25 dBm for most data presented here. We used the second IDT to detect the SAW electrically by the inverse piezoelectric effect after it had travelled $d = 2$ mm along the layer surface. Figure 2 presents an oscilloscope trace of the recorded signal (red line). The first 400 ns burst is the electromagnetic radiation. It travels with the speed of light and appears immediately at the receiver. After around $t_{trans} = \frac{d}{v_R} = 760$ ns the acoustic echo arrives. The pulsed RF allows to separate in time the electromagnetic radiation and the acoustic echo. The risetime of the acoustic echo is defined by the IDT geometry, the SAW velocity, and the burst duration²⁶.

III. RESULTS AND DISCUSSION

Figure 1(b) shows the time-resolved polarization rotation (TRPR) at 60 K for excitation SAW frequencies

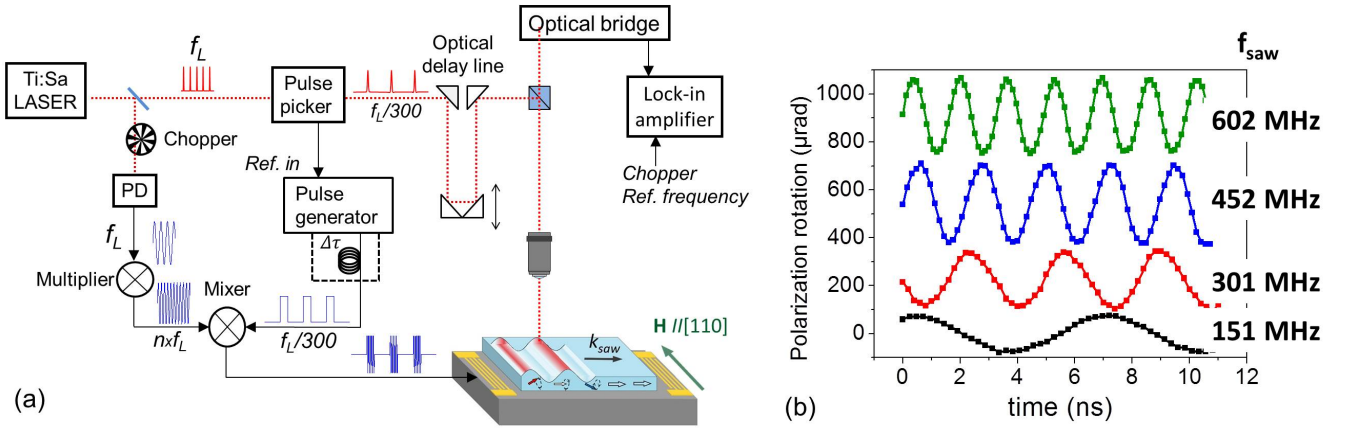


FIG. 1. (a) Schematics of the experimental set-up, (b) Time-resolved polarization rotation signal for four SAW frequencies (vertically off-set for clarity). The probe polarization was set at 60° with respect to \mathbf{k}_{SAW} . The applied magnetic field was 19.5 mT. The temperature was $T=60\text{K}$.

151, 301, 452 and 602 MHz as a function of the optical delay. The frequency of the detected signals matches exactly the excitation frequency. The amplitude of the signal varies with the magnetic field up to T_C , above which we observe only a field independent signal. This proves that the TRPR signal contains both a magnetic (field-dependent) contribution and a non-magnetic one arising from the elasto-optic effect.

In order to prove that the optically detected dynamics is indeed triggered by the SAW we monitored the amplitude of the TRPR signal at various delays after the beginning of the the RF burst by setting an electronic delay $\Delta\tau$ between the electric excitation and the optical pulse probe (Fig. 1(a)). First the probe beam was set at $100\ \mu\text{m}$ from the receiving IDT (1.9 mm from the emitter, open circle in the sample scheme of Fig. 2). The open circle symbol curve represents the amplitude of the TRPR oscillations versus the electronic delay. It has the same shape as the acoustic echo and peaks slightly before the arrival of this echo on the receiving IDT, in agreement with the location of the detection spot. Then the probe beam was positioned $67\ \mu\text{m}$ from the emitter IDT (full circle in the sample scheme of Fig. 2). The full circle curve represents the amplitude of the oscillations versus the electronic delay. It also has the same shape as the acoustic echo and is detected earlier, in agreement with the position of the detection spot. The 20% burst amplitude decrease from one burst to the other can be directly correlated to the loss of acoustic amplitude via magneto-elastic interaction, as will be seen further (Fig. 4(g)). For both spot positions, no signal is observed at the arrival time of the electromagnetic radiation. These results show that the TRPR signal is indeed generated by the SAW.

In order to disentangle the magneto-optic and the elasto-optic contributions in the TRPR signal we analyze the dependence of the signal on the probe light polarization and the applied magnetic field. The elasto-optic

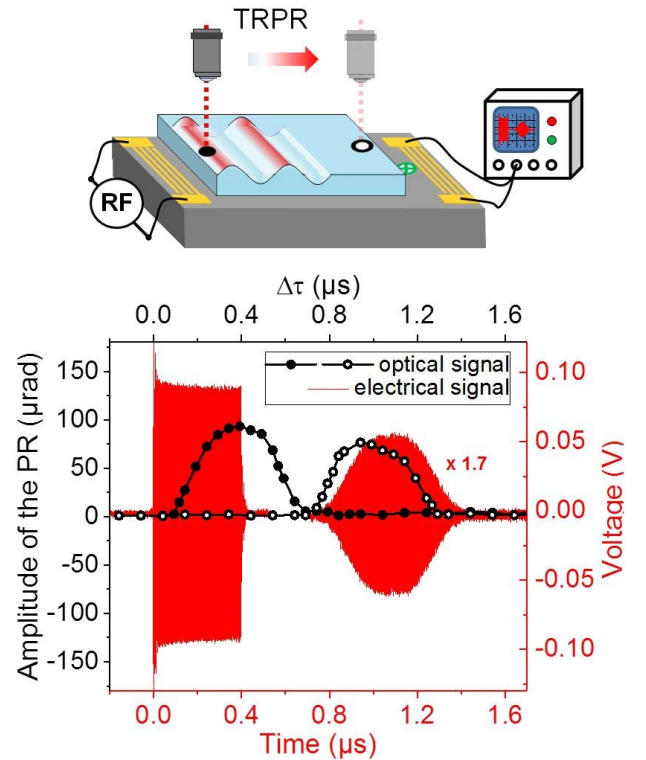


FIG. 2. Time-domain signal detected electrically (red solid line) by an oscilloscope, and amplitude of the optically detected TRPR oscillations (circles) as a function of the electronic delay. TRPR was measured in two places on the sample (open and closed symbols on the scheme). The crossed-circle symbol indicates where the optical SAW-FMR data shown in Fig. 4(h) was taken. The surface amplitudes of the excited SAW strain components are $\varepsilon_{xx} = 4.8 \times 10^{-5}$ and $\varepsilon_{zz} = 2.2 \times 10^{-5}$ estimated following the procedure described in ref.¹⁶. The SAW frequency is 452 MHz, the applied field is $\mu_0 H = 20\ \text{mT}$, the polarization angle is $\beta=30\ \text{deg}$.

effect gives rise to a dynamic birefringence with axes parallel and perpendicular to the SAW wavevector \mathbf{k}_{SAW} . The resulting rotation of linear polarization is proportional to the P_{44} component of the elasto-optic tensor of the cubic GaAs and the ε_{xx} strain component^{34–36}. It does not depend on the magnetic field. Besides we expect the contribution from two magneto-optical effects^{27,33}: the polar magneto-optical Kerr effect (PMOKE) sensitive to the out-of-plane dynamic component of the magnetization $\delta\theta$ and independent of the incoming polarization and the (weaker) Voigt effect (magnetic linear dichroism (MLD)) sensitive to the in-plane dynamic component of the magnetization $\delta\phi$ and to the field-dependent in-plane equilibrium orientation of the magnetization $\phi_0(H)$. The TRPR signal can therefore be expressed as^{26,27,33}:

$$\begin{aligned} \delta\beta &= K\delta\theta(H, t) + 2V\delta\phi(H, t) \cos(2(\beta - \phi_0(H))) \\ &\quad + P_E\varepsilon_{xx}(t) \sin 2\beta \\ &= K\delta\theta(H, t) + 2V\delta\phi(H, t) \cos 2\phi_0(H) \cos 2\beta \\ &\quad + (2V\delta\phi(H, t) \sin 2\phi_0(H) + P_E\varepsilon_{xx}(t)) \sin 2\beta \end{aligned} \quad (1)$$

where β is the angle of the probe polarization with respect to \mathbf{k}_{SAW} , K and V are the Kerr and Voigt magneto-optical coefficients, respectively, and $P_E = Re(n^3 P_{44}/(n^2 - 1))$ is the elasto-optic coefficient with n the refractive index. Indeed the experimental TRPR signal shows a clear dependence on the probe polarization (Fig. 3(a)) and on the magnetic field (Fig. 3(b)). For each time and field value, the signal is fitted as a function of β by $\delta\beta = F_\theta + G_\phi \cos 2\beta + H_{\phi\varepsilon} \sin 2\beta$. The resulting fit is very good as seen in Fig. 3(b). The offset that appears under the application of a magnetic field $\mu_0 H = 6$ mT is related to the PMOKE signal $F_\theta = K\delta\theta$. The change of the phase is a good indication of the presence of MLD. The resulting F_θ , G_ϕ , $H_{\phi\varepsilon}$ time-dependent functions are then fitted by sinusoidal functions at frequency f_{SAW} in order to extract the field-dependence of their amplitudes f_θ , g_ϕ , $h_{\phi\varepsilon}$, respectively. We have $f_\theta = K\delta\theta_0(H)$ and $g_\phi = 2V\delta\phi_0(H) |\cos 2\phi_0(H)|$ where $\delta\theta_0$ and $\delta\phi_0$ are the amplitudes of the oscillating $\delta\theta(t)$ and $\delta\phi(t)$, respectively.

In Fig. 3(c) we plot the amplitudes f_θ , g_ϕ , $h_{\phi\varepsilon}$ as a function of the applied field. The amplitude of the PMOKE signal f_θ (black curve) increases progressively to reach a maximum at 22.5 mT and then drops to zero. The MLD component g_ϕ (red curve) shows a different behavior with two maxima and a zero at $\mu_0 H = 16$ mT. The $h_{\phi\varepsilon}$ component reflecting a combination of PE and MLD (green curve) has a broad maximum and a clear 40 μrad offset owing to the field-independent elasto-optic effect.

To demonstrate that the physics of the magneto-elastic coupling is responsible for the experimental observations, the magnetization dynamics is modelled in the framework of the Landau-Lifshitz-Gilbert equation including the driving torque generated by the SAW²⁰. When the SAW is travelling along [1-10] the torque is mainly driven by the ε_{xx} strain component¹⁶. We use the sample magnetic parameters (magnetization and mag-

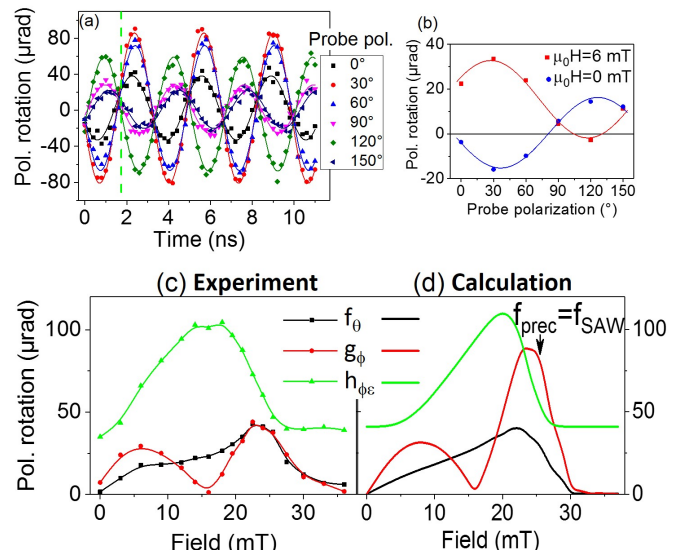


FIG. 3. Polarization and field dependence of the magnetization and strain dynamics for $f_{SAW} = 301$ MHz at $T = 60$ K. (a) TRPR signal for six polarization orientations as a function of the optical delay for $\mu_0 H = 6$ mT. (b) TRPR at fixed time delay (cross section of Fig. 3(a), green dashed line) versus probe polarization values for two field values. (c) Field variation of the three components f_θ , g_ϕ , $h_{\phi\varepsilon}$ related to polar Kerr effect (β -independent), MLD ($\cos 2\beta$ term) and mixed PE/MLD ($\sin 2\beta$ term), respectively, at $f_{SAW} = 301$ MHz. (d) Calculated amplitudes of f_θ , g_ϕ , $h_{\phi\varepsilon}$; the parameters are $K = 18$ mrad, $V = 0.8$ mrad, $P_E = 0.77$ rad with $\varepsilon_{xx} = 5.3 \cdot 10^{-5}$. The Gaussian distribution on the in-plane anisotropy constant has a standard deviation equal to 12 % of its mean value.

netic anisotropy) obtained from vibrating sample magnetometer and cavity-FMR experiments. The calculated amplitudes³⁷ of the magneto-optical signals f_θ and g_ϕ (Fig. 3(d), black and red curves, respectively) show a peak around 25 mT, corresponding to the resonance condition of equal precession and SAW frequencies at $f_{SAW} = 301$ MHz. The g_ϕ amplitude (red curve) goes to zero at a field such that the static magnetization is at 45° of the easy axis ($\cos 2\phi_0 = 0$). The baseline for $h_{\phi\varepsilon}$ is given by the PE effect that does not depend on the magnetic field. As seen from the comparison of Fig. 3(c) and (d) a good quantitative agreement between experimental and calculated f_θ , g_ϕ , $h_{\phi\varepsilon}$ curves is obtained. To account for the amplitude and width of f_θ , g_ϕ , $h_{\phi\varepsilon}$ we had to introduce a dispersion of the uniaxial in-plane magnetic anisotropy constant that is known to be crucial for SAW-induced magnetization dynamics¹⁶. These results show that we are able to disentangle the different contributions in the optical polarization signal and to accurately extract the dynamical magnetic contribution. They provide the first direct, time-domain detection of magneto-acoustic resonance induced by a *propagating* SAW. Furthermore the presence of Kerr and Voigt effects gives access to both the in-plane and out-of-plane dynamical magnetization components.

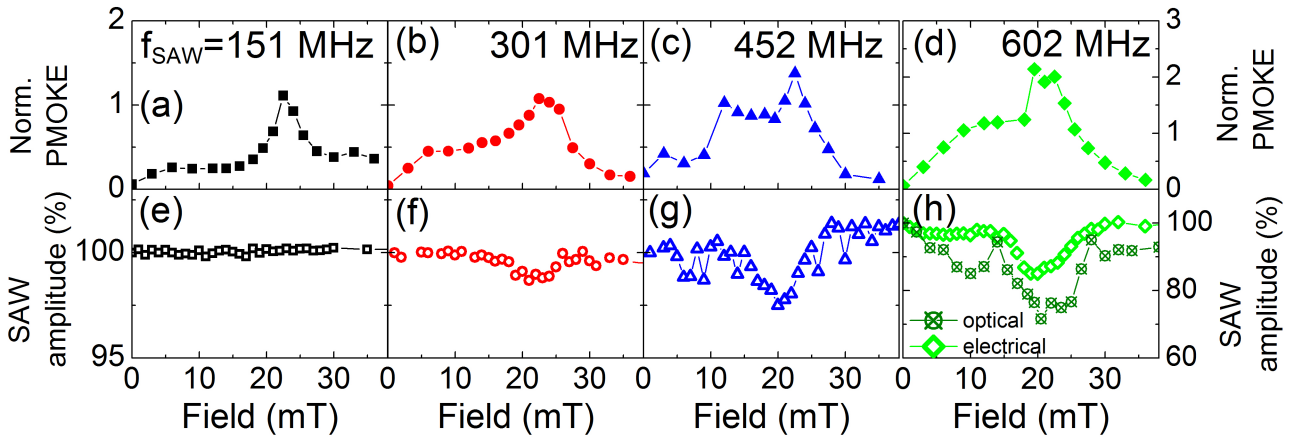


FIG. 4. Top panels: Field dependence of the PMOKE signal (out-of-plane magnetization dynamics) normalized by the field-independent photo-elastic signal for four SAW frequencies at $T=60$ K. Bottom panels: variation of the SAW amplitude with the magnetic field measured by acoustic-to-electrical conversion at the receiving IDT and in (h) normalized PE signal detected on GaAs in between the GaMnAs mesa and the receiving IDT (see crossed-circle symbol in the schematics of Fig. 2), with a polarization angle $\beta=45$ deg. The amplitudes of excited SAW strain components are estimated as $\varepsilon_{xx} = 5.3 \times 10^{-5}$ and $\varepsilon_{zz} = 1.8 \times 10^{-5}$ at $f_{SAW}=301$ MHz (they are slightly different at other frequencies but low enough to stay in the linear regime).

In order to compare the sensitivity of the magneto-optical signal detection and the SAW amplitude detection after propagation along the layer, we show in Fig. 4 the PMOKE component f_{θ} (out-of-plane magnetization dynamics) and the variation of the electrically detected SAW amplitude (through the receiving IDT) as a function of the applied magnetic field for the four SAW frequencies. The PMOKE data (top panel of Fig. 4) were normalized by the measured PE level (field-independent baseline of $h_{\phi\varepsilon}$) in order to correct for slightly different SAW amplitudes. For each frequency we observe a clear and strong peak of the PMOKE curve at the resonance field (which has close values for the four frequencies because of the steep variation of the FMR frequency with the field¹⁶). The electrically detected SAW amplitude (bottom panel of Fig. 4) is a rather noisy signal at 151, 301 and 452 MHz, with a much smaller dynamical range. At $f_{SAW} = 301, 452,$ and 602 MHz, it shows a dip at the same field as the peak of the corresponding PMOKE signal. The dip is more pronounced at the higher frequency of 602 MHz as expected from the increase of the absorbed SAW power with the SAW frequency^{1,16}. The dip is however not detectable at $f_{SAW} = 151$ MHz whereas the PMOKE peak is clearly detected. We also plot in Fig. 4(h) the amplitude of the photo-elastic signal detected on GaAs, in between the GaMnAs mesa and the receiving IDT (crossed-circle symbol in the scheme of Fig. 2), normalized by its low-field value. The data was taken for an incoming beam polarisation of 45 deg, which maximizes the strain-induced birefringence. Its field-dependence is similar to that of the electrical signal (Fig. 4(h)) in shape and amplitude. These results show the much larger dynamical range and sensitivity of the magneto-optical SAW-FMR signal, because it is detected

on a zero background, with respect to electrical or optical signal of the SAW amplitude variation, detected on a non-zero background.

IV. CONCLUSION

We have developed a sensitive time-domain optical technique to investigate the magneto-elastic coupling between piezo-electrically generated travelling SAWs and magnetization in ferromagnetic layers at variable temperature. The time-resolved magnetization precession was clearly proved to originate from the magneto-elastic coupling with the SAW and shows a resonant behavior at equal SAW and precession frequencies. Compared to the detection of the SAW attenuation, the magneto-optical time-resolved SAW-FMR signal is more sensitive and provides a better signal-to-noise ratio. The detection threshold of the time-resolved signal is mainly governed by the convolution of the SAW wavelength and the laser spot size w . As such, magnetization precession could still be observed at $f_{SAW}=900$ MHz, for which for $\lambda_{SAW} \sim 3w$. Working at higher SAW frequencies (above 1 GHz) will require a tighter focusing of the laser spot, either by working at higher photon energy (keeping a decent Kerr signal) and/or by increasing the numerical aperture of the focusing objective (keeping a good linear polarization). More generally, we believe that this approach, combining high space/time sensitivity and access to the two components of magnetization will find a wider use in any experiment requiring the synchronization of a radio-frequency electrical stimulus with the ultra-fast optical detection of the magnetic effects it induces, and should benefit broadly the magnetization dy-

namics community. Applied to magneto-strictive materials, this technique opens the way for a deeper insight into the magnon-phonon coupling and the exploration of the nonlinear regime of acoustic-wave induced magnetization dynamics.

ACKNOWLEDGMENTS

This work has been supported by the French Agence Nationale de la Recherche (ANR13-JS04-0001-01). The

authors also acknowledge D. Hrabovsky (MPBT-Physical Properties Low Temperature facility of Sorbonne Université), H. J. von Bardeleben (INSP) for magnetometry measurements, and C. Testelin (INSP) for providing scientific equipment.

-
- ¹ L. Dreher, M. Weiler, M. Pernpeintner, H. Huebl, R. Gross, M. S. Brandt, and S. T. B. Goennenwein, *Phys. Rev. B* **86**, 134415 (2012).
- ² M. Bombeck, A. S. Salasyuk, B. A. Glavin, A. V. Scherbakov, C. Brüggemann, D. R. Yakovlev, V. F. Sapega, X. Liu, J. K. Furdyna, A. V. Akimov, and M. Bayer, *Phys. Rev. B* **85**, 195324 (2012).
- ³ W. Li, B. Buford, A. Jander, and P. Dhagat, *IEEE Transactions on Magnetics* **50**, 37 (2014).
- ⁴ L. Thevenard, C. Gourdon, J. Y. Prieur, H. J. von Bardeleben, S. Vincent, L. Becerra, L. Largeau, and J.-Y. Duquesne, *Phys. Rev. B* **90**, 094401 (2014).
- ⁵ Y. Yahagi, B. Harteneck, S. Cabrini, and H. Schmidt, *Physical Review B* **90**, 140405 (2014).
- ⁶ K. Shen and G. E. Bauer, *Phys. Rev. Lett.* **115**, 197201 (2015).
- ⁷ S. Davis, J. a. Borchers, B. B. Maranville, and S. Adenwalla, *Journal of Applied Physics* **117**, 063904 (2015).
- ⁸ P. G. Gowtham, T. Moriyama, D. C. Ralph, and R. A. Buhrman, *Journal of Applied Physics* **118**, 233910 (2015).
- ⁹ P. Chowdhury, P. Dhagat, and A. Jander, *IEEE Transactions on Magnetics* **51**, 1300904 (2015).
- ¹⁰ J. Janušonis, C. L. Chang, P. H. M. van Loosdrecht, and R. I. Tobey, *Applied Physics Letters* **106**, 181601 (2015).
- ¹¹ L. Thevenard, I. S. Camara, J.-Y. Prieur, P. Rovillain, A. Lemaître, C. Gourdon, and J.-Y. Duquesne, *Physical Review B* **93**, 140405 (2016).
- ¹² L. Thevenard, I. S. Camara, S. Majrab, M. Bernard, P. Rovillain, A. Lemaître, C. Gourdon, and J.-Y. Duquesne, *Physical Review B* **93**, 134430 (2016).
- ¹³ C. L. Chang, A. M. Lomonosov, J. Janusonis, V. S. Vlasov, V. V. Temnov, and R. I. Tobey, *Phys. Rev. B* **95**, 060409 (2017).
- ¹⁴ Y. Hashimoto, S. Daimon, R. Iguchi, Y. Oikawa, K. Shen, K. Sato, D. Bossini, Y. Tabuchi, T. Satoh, B. Hillebrands, G. E. Bauer, T. H. Johansen, A. Kirilyuk, T. Rasing, and E. Saitoh, *Nat. Commun.* **8**, 15859 (2017).
- ¹⁵ J.-W. Kim and J.-Y. Bigot, *Physical Review B* **95**, 144422 (2017).
- ¹⁶ P. Kuszewski, I. S. Camara, N. Biarrotte, L. Becerra, J. von Bardeleben, W. Saverio Torres, A. Lemaître, C. Gourdon, J.-Y. Duquesne, and L. Thevenard, *Journal of Physics: Condensed Matter* **30**, 244003 (2018).
- ¹⁷ A. Lemaître, A. Miard, L. Travers, O. Mauguin, L. Largeau, C. Gourdon, V. Jeudy, M. Tran, and J.-M. George, *Applied Physics Letters* **93**, 021123 (2008).
- ¹⁸ T. K. Nath, R. A. Rao, D. Lavric, C. B. Eom, L. Wu, and F. Tsui, *Appl. Phys. Lett.* **74**, 1615 (1999).
- ¹⁹ T. L. Linnik, A. V. Scherbakov, D. R. Yakovlev, X. Liu, J. K. Furdyna, and M. Bayer, *Physical Review B* **84**, 214432 (2011).
- ²⁰ L. Thevenard, J.-Y. Duquesne, E. Peronne, H. J. von Bardeleben, H. Jaffres, S. Ruttala, J.-M. George, A. Lemaître, and C. Gourdon, *Phys. Rev. B* **87**, 144402 (2013).
- ²¹ L. Y. Yeo and J. R. Friend, *Annu. Rev. Fluid Mech.* **46**, 379 (2014).
- ²² A. V. Mamishev, K. Sundara-Rajan, F. Yang, Y. Du, and M. Zahn, *Proc. IEEE* **92**, 808 (2004).
- ²³ T. Poole and G. R. Nash, *Sci. Rep.* **7**, 1767 (2017).
- ²⁴ M. M. De Lima and P. V. Santos, *Reports Prog. Phys.* **68**, 1639 (2005).
- ²⁵ A. Neubrand and P. Hess, *Journal of Applied Physics* **71**, 227 (1992).
- ²⁶ D. Royer and E. Dieulesaint, *Elastic Waves in Solids II. Generation, Acousto-optic Interaction, Application* (Springer-Verlag, Berlin, 2000).
- ²⁷ S. Shihab, L. Thevenard, A. Lemaître, and C. Gourdon, *Physical Review B* **95**, 144411 (2017).
- ²⁸ M. Foerster, F. Macià, N. Statuto, S. Finizio, A. Hernández-Mínguez, S. Lendínez, P. V. Santos, J. Fontcuberta, J. M. Hernández, M. Kläui, and L. Aballe, *Nature Communications* **8**, 407 (2017).
- ²⁹ F. J. Schüleín, E. Zallo, P. Atkinson, O. G. Schmidt, R. Trotta, A. Rastelli, A. Wixforth, and H. J. Krenner, *Nat. Nanotechnol.* **10**, 512 (2015).
- ³⁰ R. B. Holländer, C. Müller, M. Lohmann, B. Mozooni, and J. McCord, *J. Magn. Magn. Mater.* **432**, 283 (2017).
- ³¹ M. Weiß, A. L. Hörner, E. Zallo, P. Atkinson, A. Rastelli, O. G. Schmidt, A. Wixforth, and H. J. Krenner, *Phys. Rev. Appl.* **9**, 014004 (2018).
- ³² W. Maichen, *Digital timing measurements: from scopes and probes to timing and jitter* (Springer Science & Business Media, 2006).
- ³³ P. Němec, E. Rozkotová, N. Tesařová, F. Trojánek, E. De Ranieri, K. Olejník, J. Zemen, V. Novák, M. Cukr, P. Malý, and T. Jungwirth, *Nat. Phys.* **8**, 411 (2012).
- ³⁴ D. Royer and E. Dieulesaint, *Elastic Waves in Solid I: Free and Guided Propagation* (Springer-Verlag, Berlin Heidelberg, 2000).
- ³⁵ T. Saito, O. Matsuda, M. Tomoda, and O. B. Wright, *J. Opt. Soc. Am. B* **27**, 2632 (2010).
- ³⁶ P. V. Santos, *Appl. Phys. Lett.* **74**, 4002 (1999).

³⁷ Because we are only considering the uniform FMR mode, it is unnecessary to take into account the absorption and optical phase shift of the light in the layer, as in Ref. [27].